A fully-differential biopotential amplifier with a reduced number of parts

Enrique M. Spinelli*, Pablo A. García, Federico N. Guerrero, Valentín A. Catacora and Marcelo A.Haberman

Abstract*— *Objective: **Fully differential topologies are well-suited for biopotential amplifiers, mainly for single-supply battery-powered circuits such as portable wearable devices where a reduced number of parts is desired. A novel fully differential biopotential amplifier is proposed with the goal of providing electrode offset rejection, bandwidth limitation, and a temporal response compliant with biomedical standards with only a single commercial quad operational amplifier (OA) integrated circuit.** ***Methods:*** **A novel compensation strategy was used to provide a transfer function with only one zero at the origin, which makes it easy to comply with the transient response imposed by biomedical standards. A topology with no grounded components was leveraged to obtain a common-mode rejection ratio (CMRR) ideally infinite and independent of components mismatches.** ***Results:*** **Design equations are presented and, as an example, an electrocardiogram (ECG) amplifier was built and tested. It features a CMRR of 102 dB at 50 Hz, 55 dB gain that supports DC input voltages up to ±300 mV when powered from a 0 V to 5 V single-supply voltage, and a cutoff frequency of less than 0.05 Hz with a first order response.** ***Conclusion:*** **A fully-differential biopotential front-end was designed and validated through experimental tests, demonstrating proper operation with only 4 OAs.** ***Significance:*** **The amplifier is intended for board-level design solutions, it can be built with off-the-shelf components that can be selected according to specific needs, such as reduced power consumption, low noise, or proper operation from a low-voltage power source.**

***Index Terms*—Biopotential measurement, fully-differential amplifier, low cost design.**

I. Introduction

BIOPOTENTIALS acquisition requires measuring biomedical signals with resolutions of µV while admitting DC voltages of hundreds of mV that originate in the electrode-skin interface. There are two frequently used approaches to deal with this challenge. The first is to acquire biopotentials using a high dynamic range (20 bits or more) analog-to-digital converter (ADC) and digitally remove the DC components [1]. This technique relies on high resolution Sigma-Delta ADCs or on complete digital biopotential front ends as the ADS1299 of Texas Instruments [2]. The second approach is to block DC voltages by using AC-coupled analog amplifiers and acquire with a lower resolution ADC [3][4]. In this case, an ADC of 10-12 bits is enough to obtain high quality records. These devices are usually embedded in general purpose low-power microcontrollers as ATiny85 from Microchip, MSP430FR596 from Texas Instruments, STM32L432KC from STMicroelectronics, among many others. A significant advantage for wearable low-cost systems is that a small part-count is achieved by using the embedded ADC and a reduced number of parts in the amplifier. The circuit herein proposed is intended for this latter kind of solution. For battery-powered devices, a fully-differential topology is also desired because they double the input and output voltage range of their single-ended counterparts.

AC-coupling can be implemented at the input stage, connecting the filter directly to the electrodes before amplification [4][5]. This technique blocks the electrode's dc potentials but requires the inclusion of a second AC coupled stage to reject the amplifier offset voltages and leads to large time constants in order to fulfill the transient response required by biomedical standards [4]. Moreover, Maji and Burke [6] demonstrate that as electrode impedance increases, very high input impedances are required to achieve an acceptable transient response, which could be up to the GΩ range: much higher than the 10 MΩ that IEC60601 standard demands [7].

Transient response requirements are hence best fulfilled by high common mode and differential mode input impedances (Z_C and Z_D), and a single AC-coupling stage. This can be achieved with the circuit proposed in [8], but its implementation involves 5 operational amplifiers (OAs) and two of them must have different gain-bandwidth product to achieve stable operation, thus demanding at least two different integrated circuits.

Therefore, in this paper a novel circuit that provides the aforementioned features by using four identical OAs is proposed, thus allowing its implementation with just one off-the-shelve integrated circuit (a quad OA). It provides all necessary signal conditioning for a biopotential acquisition system including high Z_C and Z_D impedances, AC-coupling,

This paragraph of the first footnote will contain the date on which you submitted your paper for review. This work was supported in part by the CONICET under Project PIP-0323, in part by the UNLP under Projects I254 and PPID/I014, and in part by the Agencia I+D+i under Project PICT 2018-03747. The authors are with the Faculty of Engineering, GIBIC, Institute of Industrial Electronics, Control and Instrumentation (LEICI), La Plata National University, La Plata 1900, Argentina, and also with the National Scientific and Technical Research Council (CONICET), Argentina, Corresponding author Enrique Spinelli (e-mail: spinelli@ing.unlp.edu.ar).

gain, and bandwidth limitation, in a compact way.

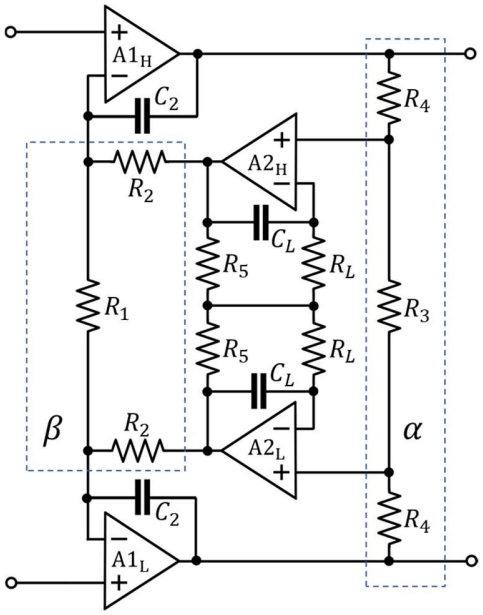

Fig. 1. Circuit diagram of the proposed biopotential amplifier. It verifies a symmetrical fully-differential structure without connections to ground.

II. Proposed Circuit

The proposed circuit is shown in Fig. 1. It is composed of a fully-differential amplifier and a fully-differential feedback circuit. The feedback circuit includes two balanced potential dividers by factors α and β encircled in dashed line in the circuit diagram, the first at the amplifier's output and the other at the amplifier's input. The originality of this topology compared with a previous published fully-differential amplifier [8] consists in the use of the balanced C_L, R_L, R_5 feedback network and the inclusion of capacitors C_2, which allow stabilizing the circuit without resorting to OAs with different open-loop gains, as will be discussed later. These capacitors also provide bandwidth limitation.

The circuit is fully-differential and symmetrical. Then, its behavior for differential and common-mode signals can be analyzed separately by using its differential and common-mode equivalent circuits [9][10], which are shown in Fig. 2 and Fig. 3 respectively.

A. Differential Mode Gain (G_{DD})

The transfer function G_{DD} for differential mode signals can be obtained by considering that the symmetry axis of the circuit is equipotential for this signal mode and representing this equipotential plane by ground connections [9]. This method produces the differential-mode equivalent circuit in Fig. 2 (a), which in turn can be simplified and represented as shown in Fig. 2 (b) yielding:

$$V_{oD} = V_{iD} - \left[V_{oD}\frac{1}{\alpha\beta}\left(1+\frac{1}{s\tau_L}\right) - V_{iD}\right]\frac{\alpha\beta}{s\tau_H}, \qquad (1)$$

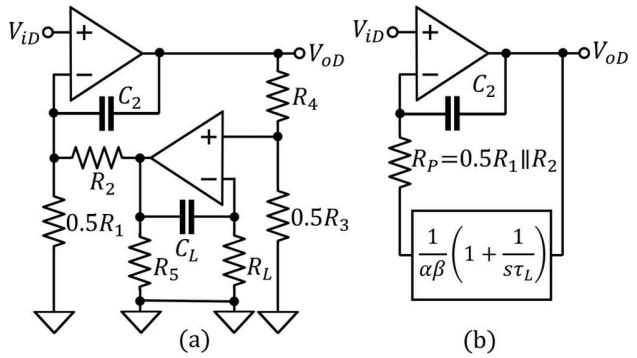

Fig. 2. (a) Differential-mode equivalent circuit and (b) its schematic representation replacing the feedback network by its transfer function.

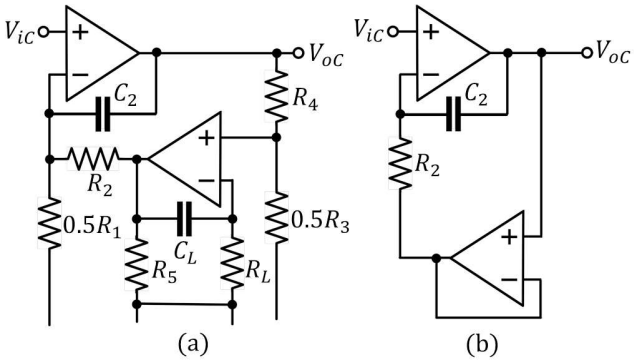

Fig. 3. (a) Common-mode equivalent circuit and (b) a simplified scheme considering that no CM current flows through R_1, R_3, R_5, and R_L.

where $\alpha = 1 + 2\,R_4/R_3$, $\beta = 1 + 2\,R_2/R_1$, $\tau_L = R_L C_L$, $\tau_H = \alpha R_2 C_2$.

The differential mode gain $G_{DD} = V_{oD}/V_{iD}$ can be obtained from (1):

$$G_{DD} = \frac{s(s + G_n/\tau_H)}{s^2 + \frac{1}{\tau_H}s + \frac{1}{\tau_L\tau_H}}, \qquad (2)$$

where G_n is the mid-frequency gain given by $G_n = \alpha\beta$. Assuming $\tau_H \ll \tau_L$, (2) can be approximated by:

$$G_{DD} \approx \frac{s(s + G_n/\tau_H)}{(s + 1/\tau_L)(s + 1/\tau_H)}. \qquad (3)$$

Further, if the amplifier gain G_n is high enough (20 dB or more), for the bandwidth of interest (3) becomes

$$G_{DD} \approx \frac{sG_n\tau_L}{(1 + s\tau_L)(1 + s\tau_H)}. \qquad (4)$$

The proposed amplifier thus presents a zero at the origin that blocks the electrodes' offset dc components, a low-cutoff frequency f_L and a high-cutoff frequency f_H given by:

$$f_L = (2\pi\tau_L)^{-1} \quad ; \quad f_H = (2\pi\tau_H)^{-1}. \qquad (5)$$

A sample frequency response for $G_n = 450$ (53 dB), $\tau_L = 4.7\ s$ ($f_L = 0.034$ Hz), $\tau_H = 680\ \mu s$ ($f_H = 234$ Hz) is shown in Fig. 4.

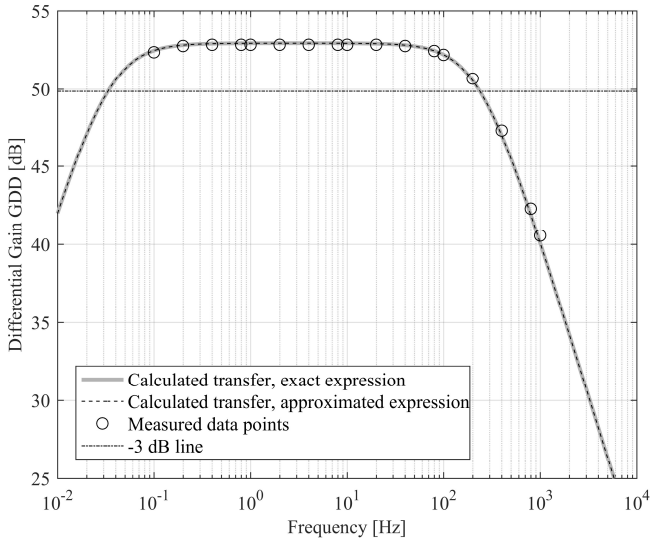

Fig. 4. The frequency response given by (2) for $G_n = 55\ dB$, $\tau_L = 4.7\ s$ ($f_L = 0.034$ Hz), $\tau_H = 680\ \mu s$ ($f_H = 234$ Hz) is shown in continuous line. Differences with the approximated expression (4), drawn in dashed line, are shown to be negligible inside the bandwidth of interest. Experimental data points are indicated with markers.

Note that resistors R_5 do not appear in the transfer functions; they are included to provide a path for bias currents of the inverter inputs of $A2_{H,L}$. A R_5 value above a few tens of KΩ is enough for this purpose, as long as it demands a low output current from the OAs.

B. Transient Response

Biopotential amplifiers must fulfill strict requirements imposed by standards such as IEC 60601 [7] AAMI [11]. The dynamic behavior is specified both by frequency response, and, most demanding, by the transient response. Indeed, the well-known maximum low cut-off frequency f_L of 0.05 Hz for ECG signals does not results from frequency response specifications but from transient response constrains [6]. The IEC 60601 standard requires that the response to a 100 ms wide 3 mV rectangular pulse presents an undershoot lower than 100 µV and a recovery slope lower than 300 µV/s [7].

For the presented topology, given that $\tau_L \gg \tau_H$, the pole $p_L = -1/\tau_L$ in the transfer function given by (4) is dominant and the input-referred amplifier transient response $y(t)$ can be approximate by a first order response that is given by

$$y(t) = 3\ \text{mV}\left(e^{-t/\tau_L} - u(t - 10\ \text{ms})e^{-(t-10\ \text{ms})/\tau_L}\right) \quad (6)$$

where $u(t)$ is the unit step function. The undershoot voltage y_U and the recovery slope m at $t = 100$ ms can be obtained from (6) resulting in [6]:

$$\begin{aligned} y_\text{U} &= y(100\ \text{ms}) = 3\ \text{mV}\left(e^{-100\ \text{ms}/\tau_L} - 1\right), \\ m &= \left.\frac{dy}{dt}\right|_{t=100\ \text{ms}} = \frac{3\text{mV}}{\tau_L}\left(e^{-100\ \text{ms}/\tau_L} - 1\right). \end{aligned} \quad (7)$$

Therefore, imposing the constrain $y_\text{U} < 100$ µV leads to $\tau_L > 3.05$ s, whereas the slope recovery limit $m < 300\ \mu\text{V/s}$ leads to $\tau_L > 1.02$ s [6]. Then, the hardest constraint is imposed by the undershoot, and a response with $\tau_L > 3.05$ s is enough to fulfill the transient response requirements for an amplifier with a first-order high-pass transfer function. In contrast, when several AC-coupled stages are cascaded, each of them contributes to the undershoot and to the recovery slope, thus demanding larger time constants to fulfill the IEC 60601 standard [4]; [6].

C. Common Mode Gain (G_{CC})

The proposed circuit does not have any connections to ground. Then, when a common-mode input voltage V_{iC} is applied at the amplifier's input, no currents flow and all nodes adopt the potential V_{iC}, including the output ones. This can be verified in the CM equivalent circuit of Fig. 3. Note that OA A2 imposes a null potential difference across the series impedance R_2-C_2. Then, no currents flow through these components and the output voltage V_{oC} equals the input voltage V_{iC} leading to:

$$G_{CC} = \frac{V_{oC}}{V_{iC}} = 1 \quad (8)$$

A unity G_{CC} gain is a desirable feature for fully differential circuits because the input common-mode voltage propagates through the stages, thus providing an appropriate operation point for all of them. For example, setting a common-mode voltage equal to $V_{CC}/2$ on the patient [12], it will appear at the input of a differential ADC at the end of the processing chain.

D. Common Mode Rejection Ratio (CMRR)

Since applying an input common-mode voltage V_{iC} produces no current flow and all nodes adopt the potential V_{iC}, the common-mode gain G_{CC} is unitary, and the differential mode output V_{oD} is null. Then, the CMRR of the proposed topology is infinite independently of component imbalance [13]. This is an ideal condition, but in practice, as occurs with the traditional two-OA fully differential amplifier, the maximum CMRR is limited by the mismatches between the CMRRs and open-loop gains of the OAs respectively [14]. Notwithstanding, a CMRR of 100 dB and above is easily achieved with this topology, even using general purpose OAs.

E. Stability

The stability of a fully-differential circuit can be analyzed by a space-state approach [15] or by using the differential-mode and common-mode equivalent circuits [9, 10,][16]. In this latter case, both equivalent circuits must be stable to ensure stability.

The differential-mode equivalent circuit is stable because all its poles are present in the transfer function G_{DD} and are in the left half-plane. However, although the CM-to-CM transfer function G_{CC} is unitary, it possesses hidden poles that correspond to non-controllable states [15] which could be unstable. One method to test stability is by introducing an initial CM condition and evaluate the circuit internal response [13], and another method is to analyze its open loop gain, as it will be herein done.

The open loop gain (GH_{CC}) for the common-mode equivalent circuit can be obtained from the schematic of Fig. 3 (b). Connecting V_{iC} to ground and opening the loop at the input of A2, the transfer function results:

$$GH_{CC}(s) = \frac{A(s)}{1 + A(s)} \frac{1}{sR_2C_2}. \quad (9)$$

The first factor corresponds to the operational amplifier A2 working as unity-gain buffer, and the second to the integrator composed by A1, R_2 and C_2.

Following (9), R_2 and C_2 can be configured to obtain a response leading to a stable closed-loop system. Fig. 5 shows a Bode plot where the unity-gain buffer transfer function is indicated in gray and the overall GH_{CC} given by (9) in black. The buffer transfer function is close to unity for frequencies below the Gain-Bandwidth Product (GBP_{OA}) of the operational amplifier. Then, stability is easy to ensure by selecting a time constant $\tau_2 = R_2C_2$ that defines an integrator unity gain cut-off frequency $f_2 = (2\pi R_2C_2)^{-1}$ much lower than GBP_{OA} (i.e. a decade). In this way, GH_{CC} crosses the 0 dB line with 20 dB/dec slope and the phase margin is 90º. The condition for stability can thus be expressed as:

$$(2\pi R_2C_2)^{-1} < GBP_{OA}/10 \quad (10)$$

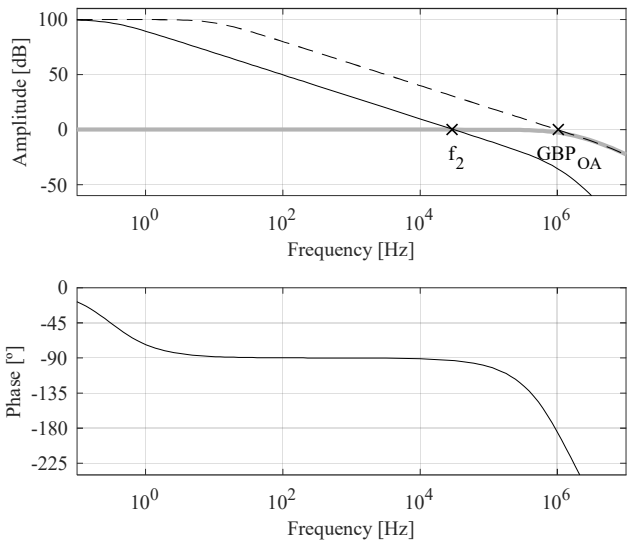

Fig. 5. Open-loop transfer function GH_{CC} for CM voltage (in black). The OA open-loop gain is marked in dashed line, and the transfer function of the unity gain buffer in gray. The latter corresponds to the first factor in (9).

F. Maximum DC Input Range

The input DC component is actively cancelled by the action of the amplifiers $A2_H$ and $A2_L$, which must act through the divider factor β to reach the input. If they are rail-to-rail amplifiers the maximum DC component that each can output is V_{CC}. Therefore, considering the differential signal and attenuation leads to:

$$V_{iDC,MAX} = \pm V_{CC}/\beta \quad (11)$$

G. Equivalent Input-Referred Noise

The overall amplifier noise is mainly due to the contributions of $A1_H$, $A1_L$ and the resistor R_1. As in [8], the noises of $A2_H$ and $A2_L$ are attenuated by the factor β, and the same occurs for the noise of the AC network R_L, C_L which is not significant inside the bandwidth of interest [17]. The Power Spectral Density (PSD) of the output voltage noise is given by:

$$E_o^2(f) = \left(4kTR_1 + 2E_{A1}^2(f)\right)|G_{DD}(f)|^2, \quad (12)$$

where $E_{A1}^2(f)$ is the voltage noise PSD of $A1_H$ and $A1_L$; k is the Boltzman's constant, and $G_{DD}(f)$ is the differential mode amplifier transfer function given by (2). Referring this PSD to the input results in

$$E_i^2(f) = 4kTR_1 + 2E_{A1}^2(f). \quad (13)$$

If power consumption is not an issue, a low value R_1 resistor can be adopted, and its contribution neglected. For reference, a 6 kΩ resistor exhibits a thermal noise of 10 nV/$\sqrt{\text{Hz}}$, which is comparable to that of a low noise CMOS operational amplifier. Then, keeping R_1 below this value, the overall noise is dominated by the contributions from $A1_H$ and $A1_L$:

$$E_i^2(f) \approx 2E_{A1}^2(f) \quad (14)$$

H. Design Example

As an example, an ECG biopotential amplifier was designed with the following specifications: 0 V-5 V power-supply; high-pass cut-off frequency $f_L < 0.05$ Hz; low-pass cut-off frequency $f_H > 150$ Hz and a DC input range $V_{iDC,MAX} > \pm 300$ mV. The amplifier must provide a differential output voltage $V_{oD} \leq \pm 2.5$ V for an AC input range $V_{iAC,MAX} = \pm 5$ mV, thus imposing a gain G_n below 500 times. Given these requirements, the amplifier design procedure is sequential and is described as follows:

1. The factor β is set according to (11) as:

$$V_{iDC,MAX} = \pm V_{CC}/\beta \geq \pm 300 \text{ mV} \quad (15)$$

To achieve $V_{iDC,MAX} \geq \pm 300$ mV with $V_{CC} = 5$ V a $\beta \leq 16.6$ is needed. Using $R_2 = 22$ KΩ and $R_1 = 3.3$ KΩ yields $\beta = 14.3$ and $V_{iDC,MAX} \approx \pm 350$ mV.

2. The factor α is calculated to achieve the required gain:

$$G_n = \alpha\beta \leq 500 \quad (16)$$

For $\beta = 14.3$, α must be lower than 34.8. Adopting $R_4 = 33$ KΩ and $R_3 = 2.2$ KΩ results in $\alpha = 31.0$ and an overall gain $G_n \approx 450$.

3. The time constant R_LC_L is set according to (5) to fulfill a high-pass frequency $f_L < 0.05$ Hz :

$$\tau_L = R_LC_L > \frac{1}{2\pi 0.05} = 3.2\ s \quad (17)$$

$R_L = 4.7$ MΩ, $C_L = 1$ µF yield $\tau_L = 4.7\ s$ and $f_L = 0.034$ Hz.

4. The time constant τ_H is set according to (5) for a high cut-off frequency $f_H > 150$ Hz.

$$\tau_H = \alpha R_2 C_2 < \frac{1}{2\pi 150\ \text{Hz}} = 1.1\ \text{ms} \qquad (18)$$

Considering $\alpha = 31.0$ leads to $R_2 C_2 < 34$ µs. For $R_2 = 22$ KΩ (designed in the first step) then $C_2 < 1.6$ nF. Finally, $C_2 = 1.0$ nF was adopted thus setting $\tau_H = \alpha R_2 C_2 = 682$ µs and $f_H = 1/(2\pi\alpha R_2 C_2) = 233$ Hz.

III. Experimental Results

The designed biopotential amplifier was built and tested using the Texas Instruments TLC2274 quad OA. The complete circuit is shown in Fig. 6. Note that electrode E3 is connected to 2.5 V to provide a proper common-mode voltage for single-supply operation. For the bench tests, its differential output was connected to an INA111 instrumentation amplifier from Texas Instruments with a gain of 51 times, which provided a single-ended output that allows measuring with standard instruments.

A. Frequency Response

The amplifier frequency response is shown in Fig. 4. The measurements were performed by an Agilent DSO-X 2024A digital oscilloscope working in averaging mode (32 frames). As can be observed in these figures, the responses verify the requirements of the IEC standard [7].

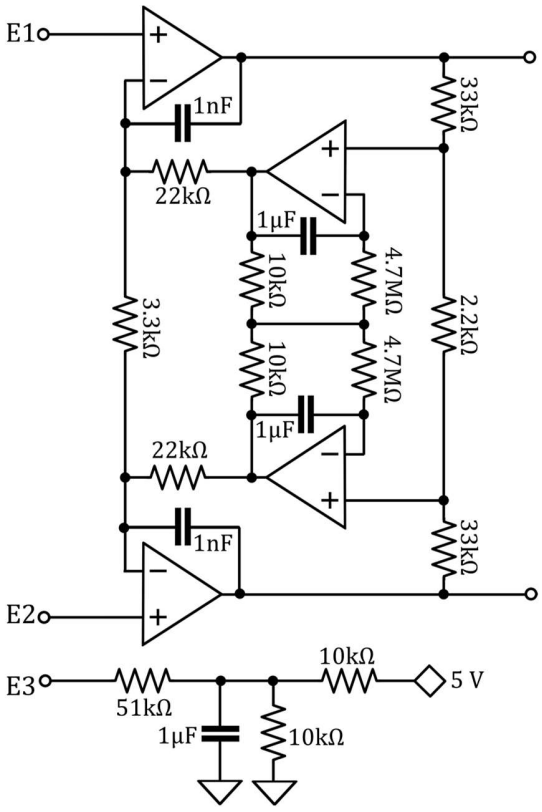

Fig. 6. Complete circuit of the proposed biopotential amplifier used in the experimental test.

B. Common Mode Rejection Ratio (CMRR)

The CMRR of the amplifier was measured applying a common mode voltage of 1 V_{PP} with a DC offset of 2.5 V. The CMRR @50 Hz is 101 dB, and approximately constant with a mean value of 100.8 dB for frequencies between 1 Hz-1 kHz.

C. Transient Response

The response to a 3 mV square pulse of 10 ms according to the IEC 60601 standard was obtained. As can be observed in Fig. 7, the transient response presents an undershoot lower than 100 µV and a recovery slope lower than 300 µV/s.

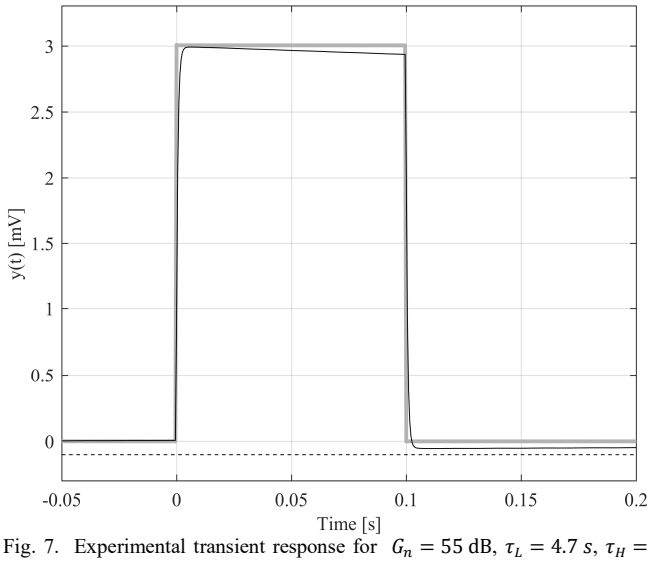

Fig. 7. Experimental transient response for $G_n = 55$ dB, $\tau_L = 4.7\ s$, $\tau_H = 680$ µs. The maximum admissible undershot of 100 µV is indicated in dashed line. The output $y(t)$ is referred to the input.

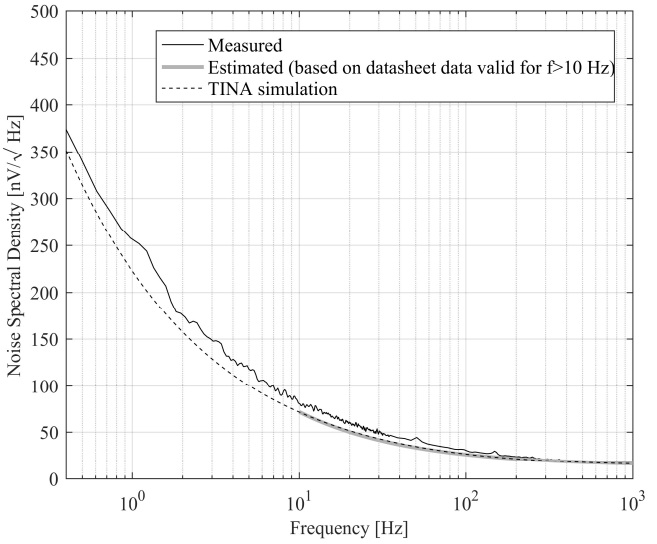

Fig. 8. Amplifier noise spectral density (PSD). In black: experimental PSD; in dashed line: simulation results; in gray: PSD predicted by (13) using the OA noise specified in its datasheet (only specified above 10 Hz).

D. Amplifier Noise

The amplifier input-referred noise is shown in Fig. 8. The experimental noise power spectral density (PSD), indicated in

continuous black line, was measured with a Stanford Research SR760 spectrum analyzer. A simulation result obtained using TINA SPICE software from Texas Instruments is also shown in dashed line, and finally, in thick gray line, the PSD predicted by (13) using the PSD OA noise reported in the TLC2274 datasheet for frequencies above 10 Hz. This latter curve shows a good agreement with experimental data and simulation results, thus validating (13).

E. Acquisition of Electrocardiographic (ECG) Signals

The amplifier was tested acquiring real ECG signals. For this purpose, it was connected to a previously designed wireless configurable acquisition platform [18] that admits differential input signals. Standard disposable Ag/AgCl electrodes were placed according to derivation I to obtain the records shown in Fig. 9.

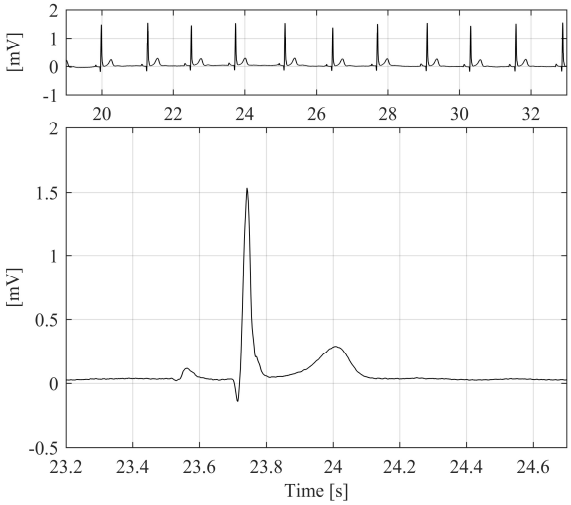

Fig. 9. ECG record acquired with the proposed biopotential amplifier.

IV. Conclusion

A novel biopotential amplifier that can be built with just one quad operational amplifier integrated circuit was proposed. It provides amplification, high common-mode and differential-mode input impedances, DC electrode offset rejection, and bandwidth limitation, thus covering all signal conditioning tasks of a biopotential acquisition system while maintaining a reduced number of parts. Its output is differential, in line with current ADC tendencies. The design equations as well as the design process are simple, including stability considerations. The CMRR of the amplifier does not depend on component tolerances and can easily reach 100 dB at power line frequencies. As an example and experimental validation, an ECG amplifier was designed, built, and tested. It exhibited a gain of 55 dB, a CMRR of 101 dB at 50 Hz and its frequency and transient response met the requirements of IEC 60601. The circuit does not rely on specific integrated circuits but on general-purpose ones, thus providing independence for manufacturers and alternatives in front of IC provision issues.

References

[1] J. J. McKee et al, "Sigma-delta analogue-to-digital converters for ECG signal acquisition," in *Proc. 18th Ann. Int. Conf. IEEE Eng. Med. Biol. Soc.*, 1996, pp. 19–20.

[2] *ADS1299-x low-noise, 4-, 6-, 8-channel, 24-bit, analog-to-digital converter for EEG and biopotential measurements*, Texas Instruments, Dallas, TX, 2012.

[3] J. Xu et al., "Review of bio-amplifier architectures," in *Low Power Active Electrode ICs for Wearable EEG Acquisition*. Cham, Switzerland: Springer, 2018, pp. 11–21.

[4] E. M. Spinelli et al., "AC-coupled front-end for biopotential measurements," *IEEE Trans. Biomed. Eng.*, vol. 50, no. 3, pp. 391–395, Mar. 2003.

[5] M. J. Burke and D. T. Gleeson, "A micropower dry-electrode ECG preamplifier," *IEEE Trans. Biomed. Eng.*, vol. 47, no. 2, pp. 155–162, Feb. 2000.

[6] S. Maji and M. J. Burke, "Establishing the input impedance requirements of ECG recording amplifiers," *IEEE Trans. Instrum. Meas.*, vol. 69, no. 3, pp. 825–835, Mar. 2020.

[7] *Medical electrical equipment — Part 1-11: General requirements for basic safety and essential performance — Collateral standard: Requirements for medical electrical equipment and medical electrical systems used in the home healthcare environment*, IEC 60601-1-11:2015, Jan. 2015.

[8] E. M. Spinelli et al., "A novel fully differential biopotential amplifier with DC suppression," *IEEE Trans. Biomed. Eng.*, vol. 51, no. 8, pp. 1444–1448, Aug. 2004.

[9] R. D. Middlebrook, *Differential Amplifiers*. New York: Wiley, 1963.

[10] S. A. Witherspoon and J. Choma, "The analysis of balanced, linear differential circuits," *IEEE Trans. Educ.*, vol. 38, no. 1, pp. 40–50, Feb. 1995.

[11] *ANSI/AAMI EC11-1991 - Diagnostic Electrocardiographic Devices*, IEEE 1426-1996, 2007.

[12] E. M. Spinelli et al., "A single supply biopotential amplifier," *Med. Eng. Phys.*, vol. 23, no. 3, pp. 235–238, Jun. 2001.

[13] E. M. Spinelli et al., "A design method for active high–CMRR fully–differential circuits", *Int. J. Instr. Tech.*, vol. 1, no. 2, pp. 103–113, Apr. 2013.

[14] R. Pallás-Areny and J. G. Webster, "Common mode rejection ratio in differential amplifiers," *IEEE Trans. Instrum. Meas.*, vol. 40, no. 4, pp. 669–676, Aug. 1991.

[15] E. M. Spinelli et al., "Independent common-mode and differential-mode design of fully differential analog filters," *IEEE Trans. Circuits Syst. II: Express Br.*, vol. 53, no. 7, pp. 572–576, Jul 2006.

[16] P. J. Hurst and S. H. Lewis, "Determination of stability using return ratios in balanced fully differential feedback circuits," *IEEE Trans. Circuits Sys. II: Analog and Digital Sig. Process.*, vol. 42, no. 12, pp. 805–817, Dec. 1995.

[17] E. M. Spinelli and M. A. Haberman, "Noise analysis of fully differential circuits," *IEEE Lat. Am. Trans.*, vol. 10, no. 4, pp. 1889–1892, Jun 2012.

[18] P. A. García et al., "A versatile hardware platform for brain computer interfaces," in *2010 IEEE Ann. Int. Conf. IEEE Eng. Med. Biol.*, 2010, pp. 4193–4196.